Project 2

DEVICE TO MEASURE DRAG FORCE IN A WIND TUNNEL

December 14, 2017

ME 362, Section 1

Dr. Scott Thomson

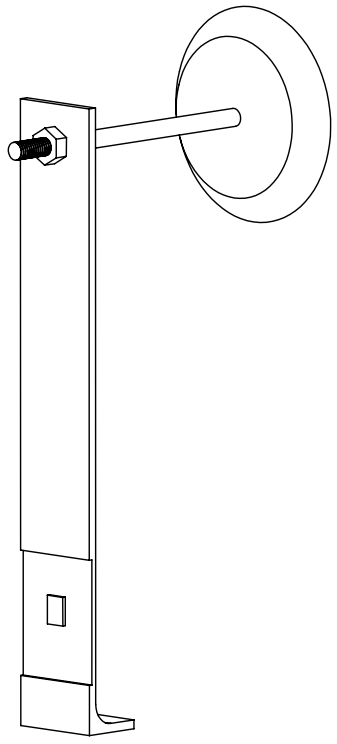

Andrew Torgesen

Abstract

The drag coefficient, C_D, of a flat disk and rectangular bar are measured and expressed as a function of the Reynolds number, Re, using a custom-built measurement device mounted in a wind tunnel. An established method for data acquisition is applied using signal conditioning and calibration of the measurement system with known loads. Drag is then measured at different wind speeds. It is found that the constructed measurement device is more accurate and less sensitive to uncertainties when subjected to higher air flow velocities. Several recommendations are made, including using a different material, using specialized measuring devices, and securing the measurement device and attached wires securely.

1 Introduction

Empirically, it has been shown that the drag coefficient of an object can be expressed as a function of Reynolds number. Knowledge of an object's drag coefficient reveals the drag force which will be induced when placing the object in various flow conditions. This relationship can be reverse-engineered in a wind tunnel by recording the drag force on an object at various air flow conditions. The use of a wind tunnel allows for precise control over flow conditions. Obtaining accurate drag force data requires the use of a separate device capable of measuring unidirectional forces on the order of 0-10 Newtons (for small objects).

A reliable force-sensing device must have a sufficient static sensitivity to register small force perturbations, while also attenuating possible sources of noise. The uncertainties inherent in the measurement device's output must be known and well-documented. Above all, the device's force output in a wind tunnel must concur with established drag data for well-known object shapes.

2 Objectives

The principle objective of this project was to construct a device capable of measuring drag force to calculate an object's drag coefficient within 10% accuracy, all with an acceptable level of uncertainty. The accuracy of the device would be verified against known drag coefficient data for a flat disk. The secondary objective of this project was to use our newly constructed measurement device to estimate the drag coefficient of an object of our choice—in this case, a rectangular bar.

3 Theory and Background

3.1 Drag Force and Coefficient of Drag

When an object is subjected to surrounding fluid flow, a drag force is induced on the object in the direction of the flow. The drag force, $\mathcal{D}$, can be calculated using the following formula:

$$\mathcal{D} = 1/2 \ \rho \ v^2 \ A \ C_D, \tag{1}$$

where ρ is the density of the flowing fluid, v is the flow velocity, A is the cross-sectional area of the object perpendicular to the flow, and C_D is the object's coefficient of drag. If $\mathcal{D}$ can be measured directly, then equation 1 can be rearranged to solve for C_D.

3.2 Strain in Cantilever Beams

When a cantilever beam undergoes linear elastic deformation due to a point load on its free end, the relationship between strain at the beam's fixed end, ϵ, and the magnitude of the point load, F, can be expressed as follows:

$$F = \frac{w \ t^2 \ E}{3 \ l} \ \epsilon, \tag{2}$$

where w is the beam's width, t is the beam's thickness, l is the beam's length, and E is the modulus of elasticity of the beam's material. For small beam deflections, w, t, l, and E can all be treated as constants, making the relationship between F and ϵ linear. Thus, if a strain gauge is mounted at the fixed end of the beam, then F can be directly related to the strain gauge's voltage output through a calibration routine.

3.3 Propagation of Uncertainty

Measurement systems inherently have uncertainty associated with their output. Uncertainty in a system arises from factors such as random Gaussian noise, the measurement and calibration procedures used, limitations in output resolution. If a parameter, x, is functionally dependent on multiple independent parameters, x_i, then the uncertainty of each independent parameter, u_T, propagates to the uncertainty of the dependent parameter, u_i, according to the following formula:

$$u_T = \sqrt{\sum_i (\frac{\partial x}{\partial x_i} \ u_i)^2}. \tag{3}$$

4 Method

4.1 Measurement Device Design and Construction

For our measurement device, we decided to construct an upright cantilever beam with a single strain gauge mounted near the base. The beam was constructed out of aluminum, and the strain gauge was hand-mounted with super glue. In order to increase the static sensitivity of the system in response to beam deflections, we thinned out the region where a single strain gauge was mounted. This allowed for a greater strain range with respect to the applied force. We did not anticipate the introduction of significant temperature expansion biases in our measurement device, so we felt justified in using only one strain gauge with a quarter-bridge Wheatstone bridge configuration. Device dimensions are provided in Fig. 4.1.

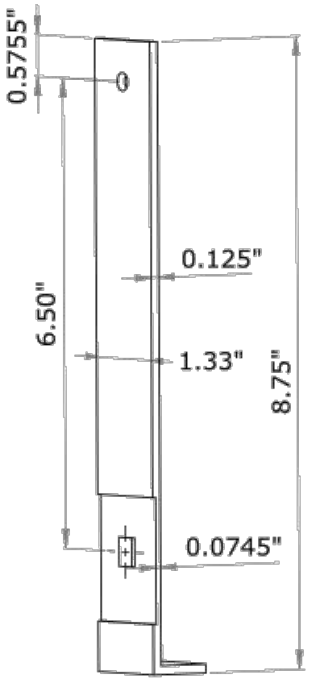

Figure 4.1: Measurement device dimensions.

We constructed the measurement device out of a stock bar of aluminum. The bar was bent at one end to allow for it to be clamped onto the base of the wind tunnel. A hole was drilled on the other end to attach a different drag object for each measurement trial. The strain gauge region was thinned out using a grinding wheel.

4.2 Measurement Device Calibration

Our calibration process consisted of three steps:

1. Linear Fitting
2. Standing Bias Calculation
3. Dynamic Bias Calculation

(a): Step 1

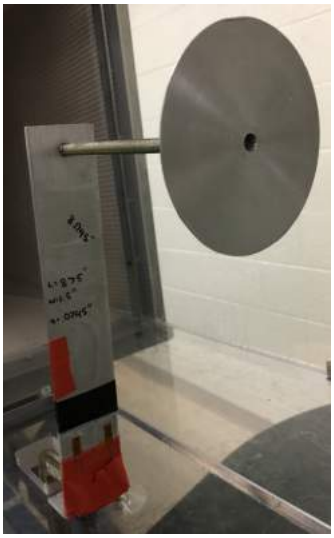

(b): Step 2

(c): Step 3

Figure 4.2: Steps for calibration. The measuring device positions represent the steps taken to derive a conversion between strain gauge voltage output and applied force (a), measure the standing force of the attached drag object (b), and measure the drag force on the measurement device without a drag object (c).

Linear fitting consisted of laying the measurement device flat and placing 300g, 500g, and 600g weights on the end (see Fig. 4.2a). Using 850 output voltage samples for each weight, we constructed a linear calibration curve which allowed us to obtain a direct relationship between strain gauge voltage and force. The linear fit gave us a static sensitivity coefficient, F_k, and a calibration bias, F_b. The linear calibration fit can be seen in Fig. 4.3.

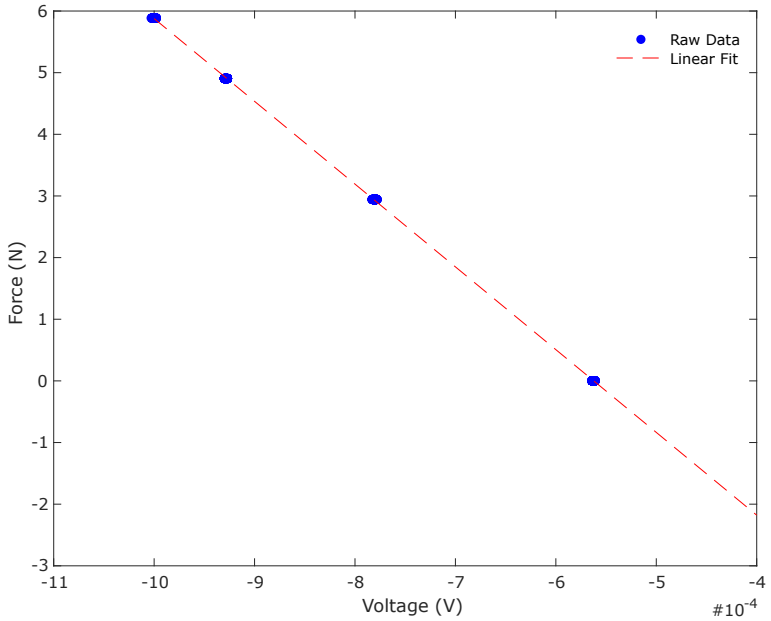

Figure 4.3: Calibration curve using various weights. 850 raw data values were used for each weight measurement. From this data we obtained the static sensitivity, $F_k = -13427\ N/V$, and offset, $F_b = -7.549\ N$.

Static bias calculation consisted of measuring the strain gauge voltage output, V_2, with the measurement device upright and the drag object attached (see Fig. 4.2b). For dynamic bias calculation, we placed the measurement device in the wind tunnel without a drag object attached (see Fig. 4.2c), then measured the voltage outputs, V_i, at fan speeds of 10, 20, 30, 40, and 50 hz. This allowed us to account for the drag force on the measurement device itself.

Using our calibration values and measurement device data, we derived a linear equation to calculate the force felt on a drag device at different velocities in the wind tunnel. If V_1 is the voltage measured during the data acquisition processes for fan speed i, then the drag force on the drag object, F_{obj}, could be calculated with the following equation:

$$F_{obj} = (V_1 - V_2 - V_i)\ F_k + F_b. \tag{4}$$

4.3 Experimental Data Acquisition

We used our calibrated measurement device to obtain drag force data on two different drag objects: a flat disk and a rectangular bar. The drag force on each object was measured inside the wind tunnel at fan speeds of 10, 20, 30, 40, and 50 hz. Measurements taken with the flat disk attached will be referred to collectively as the flat disk trial, and measurements

taken with the rectangular bar attached will be referred to as the rectangular bar trial. For each trial, the measurement device was clamped to the bottom of the wind tunnel chamber and aligned with the direction of air flow, as shown in Fig. 4.4.

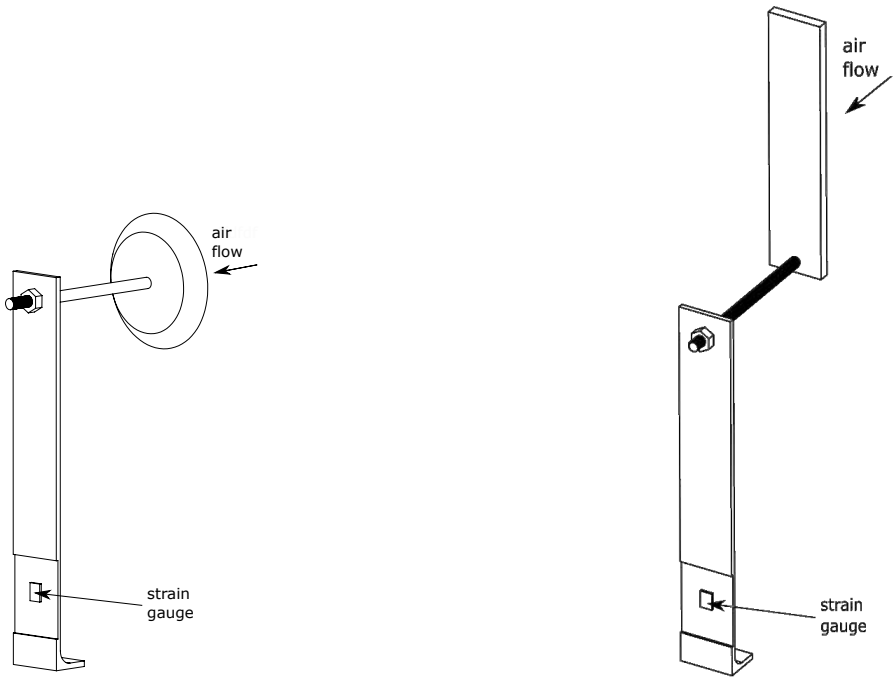

(a): Flat disk trial. *(b): Rectangular bar trial.*

Figure 4.4: Measurement device configurations for the two measurement trials. The calibrated strain gauge measures the applied drag force from and in the direction of air flow.

To measure the voltage output of the strain gauge, we used a LabVIEW data acquisition setup. The corresponding block diagram is shown in Fig. A.1. We utilized the NI 9982 Wheatstone bridge adapter, shown in Fig. A.2, to expand the output voltage range to $0 - 120\ V$ and simultaneously filter the signal. We acquired data at a rate of 500 hz and resolution of $7.153 * 10^{-6}\ V$.

Conversion between fan speed and air flow velocity was performed using the following calculation, provided in the wind tunnel documentation:

$$y = 0.819x - 0.632, \tag{5}$$

where x is the wind speed in hz, and y is the air flow velocity in m/s. Air density was calculated using a measured pressure of 652.5 mmHg and a temperature of 296.15 K.

4.4 Uncertainty Analysis

Uncertainty in the measured drag force and coefficient of drag was evaluated using advanced stage uncertainty analysis. Uncertainty of the strain gauge output voltage was calculated using the root-sum-square of the strain device instrument uncertainty, digital-to-analog converter zero$^{\text{th}}$-order uncertainty, and the uncertainty due to noise. Uncertainty in the coefficient of drag was calculated using an engineering estimate of propagation of uncertainty, as described in Section 3.3. Detailed uncertainty calculations can be found in the Appendix, in Fig. A.3 and Fig. A.4.

Uncertainty of the force measurement was reduced by recording at least 850 data points after the voltage response reached steady state for every calibration and data acquisition trial. 95% confidence intervals for both the noise and instrument uncertainty were constructed using the Student's t-distribution. Taking at least 850 data points amounted to a large sample size, which reduced the uncertainty.

Measured parameters influencing the coefficient of drag included the measured pressure, temperature, wind velocity, drag force, dimensions of the drag objects, and propagation of uncertainty to the cross-sectional area of the drag objects. The values of uncertainty all included a zero$^{\text{th}}$-order uncertainty and instrument error. Since we did not have data for the instrument uncertainty of the each measurement device, we use a value of 5% as an estimate. Measurement devices used included a mercury barometer (resolution of 1 mmHg), an alcohol glass thermometer (resolution of 1° C), a frequency of wind tunnel fan rotation (resolution of 0.1 Hz), a measuring tape (resolution of 1/16$^{\text{th}}$ of an inch), and a digital caliper (resolution of 0.001 inches).

5 Results and Discussion

The calculated drag coefficient results in significant uncertainty for the lowest wind velocities (See Table 1). As the wind velocity increases the uncertainty of this non-dimensional number gradually decreases. This is due to propagation of uncertainty that this is maximized when the velocity term of the coefficient of drag equation is small. If all other parameters are certain, the total uncertainty will still be proportional to the wind velocity. Because the uncertainty of the bar does not decrease at the same rate as the uncertainty using the disk, other parameters do contribute to the overall uncertainty in Table 1.

Parameters influencing uncertainty of the calculated coefficient of drag are the force on the beam, measured atmospheric pressure, ambient temperature, and the cross sectional areas of the objects. Each of these parameters can be measured more accurately with more

Table 1: Uncertainty of measured drag and coefficient of drag for both the disk and bar. Values for coefficient of drag and wind velocity uncertainties vary with wind tunnel velocity, as indicated.

	7.56 m/s	**15.57** m/s	**23.94** m/s	**32.13** m/s	**40.32** m/s
Uncertainty of $C_{d,disk}$	5.4993	0.9062	0.4848	0.3525	0.2944
Uncertainty of $C_{d,bar}$	4.7664	0.8088	0.4638	0.3648	0.3259
Uncertainty of Wind Velocity (m/s)	0.2785	0.6136	0.9488	1.2842	1.6195

precise equipment. For example, atmospheric pressure is more precisely measured using an instrument with an electronic display. Though analog measurements can result in relatively small uncertainty. The uncertainty of the disk cross sectional is only 0.25% of the total area. However the uncertainty of the pressure measurement is 5% of the measured value.

Table 2: Uncertainty of several measured system parameters. These values contribute to uncertainty in the coefficient of drag.

	Drag (N)	**Pressure (kPa)**	**Temperature (K)**	**Area of Disk m^2**	**Area of Bar m^2**
Uncertainty	0.3598	4.350	1.3000	1.161e-05	9.6348e-06

Uncertainty in the coefficient of drag was increased greatly by the propagation of uncertainty of the wind speed velocity, air pressure, and measured drag. These terms in the root-sum-square of the propagation of error equation were calculated to have a numerical value between two and four at a wind speed velocity of 7.67 m/s. At the same wind speed, temperature and cross-sectional area were calculated to have a numerical value less than one. The large uncertainty in the coefficient of drag for a wind speed of 7.67 m/s pointed to intrinsic limitations of the measurement system at low wind velocities. Changes in the strain gauge voltage output in this region were very small.

Having obtained calibrated drag force data for both the flat disk and rectangular bar trials, we plotted the forces against the calculated wind tunnel velocities (see Fig. 5.1). We compared the flat disk force-velocity data to previous data we obtained from a similar test using different equipment (see Fig. 5.2). In the test corresponding to Fig. 5.2, we used the same wind tunnel and flat disk, but with a pitot probe, pressure transducer, force transducer, barometer, and a specialized measuring device purchased by the school that provided more accurate data.

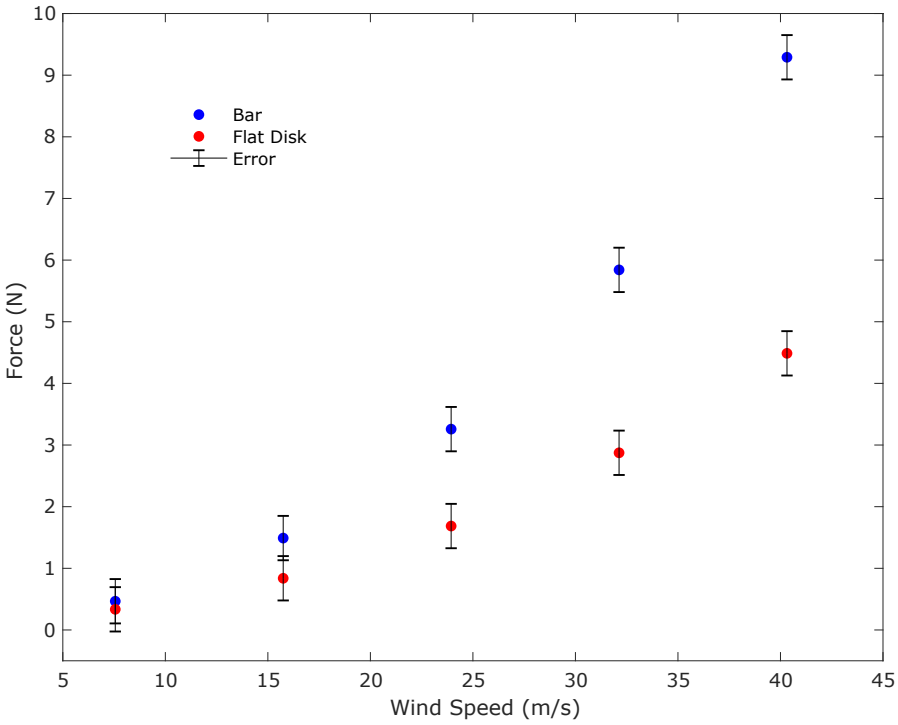

Figure 5.1: Dimensional drag data (force [N] vs. wind speed [m/s]) for both the bar and flat disk with our measurement device. Error bars from uncertainty calculations are included with each point.

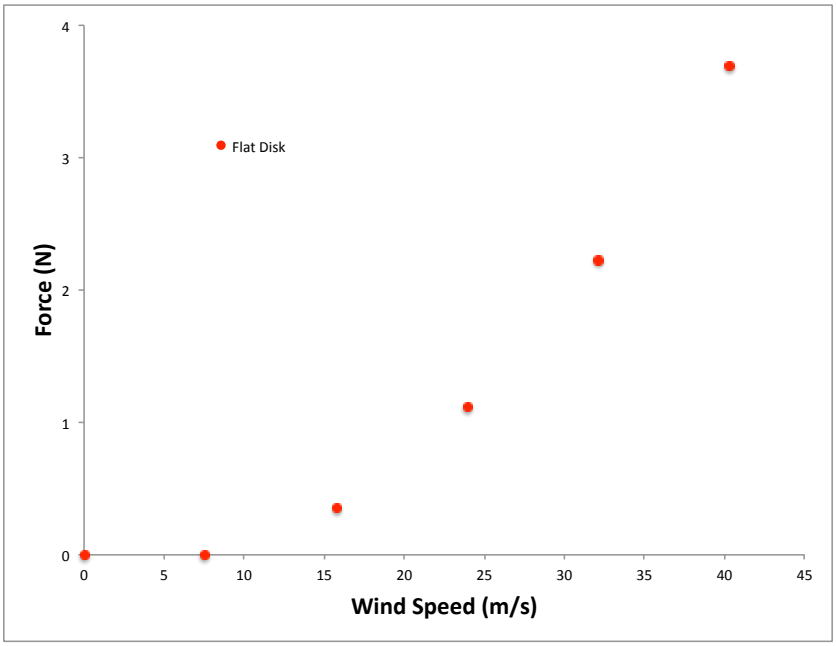

Figure 5.2: Dimensional drag data (force [N] vs. wind speed [m/s]) the flat disk with the purchased measurement device. Error bars from the data are unavailable.

Comparing Fig. 5.1 and Fig. 5.2, it is evident that the measured forces at higher velocities

were relatively larger on our constructed measurement device. This is partially because of how we designed our measuring device, thinning out the lower section where the strain gauge was attached. Some of the equations we used in our analysis, such as Eqn. 2, assume uniform thickness across the beam. Also, the thickness of our thinned-out section was smaller than that of the school-purchased measurement device. In Fig. 5.2, the force at 7.56 m/s is zero. This was due to the stiction of the purchased device, which required a force greater than a certain threshold to register change. At 7.56 m/s, the wind tunnel did not reach this necessary force threshold. On the other hand, our designed measurement device had much lower stiction threshold and registered a small force around 0.25 N at 7.56 m/s. This small difference of force slowly grew as the wind tunnel velocity increased. This difference could have come from small, inelastic deformation that occurred in the measurement device after each use, along with the movement of the testing equipment to each area within the lab. After some investigation, we found that there was a small measurement bias difference between each LabVIEW data acquisition assistant; we used had used one assistant for calculating V_1 and V_2, and another for V_i. One final possible culprit for force inaccuracies has to do with the stability of our measurement device as it was mounted to the beam. At fan speeds above 20 hz, there came to be significant oscillations in our measurement device, rapidly changing the device's orientation with respect to the direction of air flow. It is possible that such oscillations led to a level of resonance, slightly increasing the magnitude of the measured force.

With the values obtained for each trial as described in Section 4.3, we generated non-dimensional drag data and plotted it in Fig. 5.3. This plot was created using calculated values for each drag object's drag coefficient and Reynolds number.

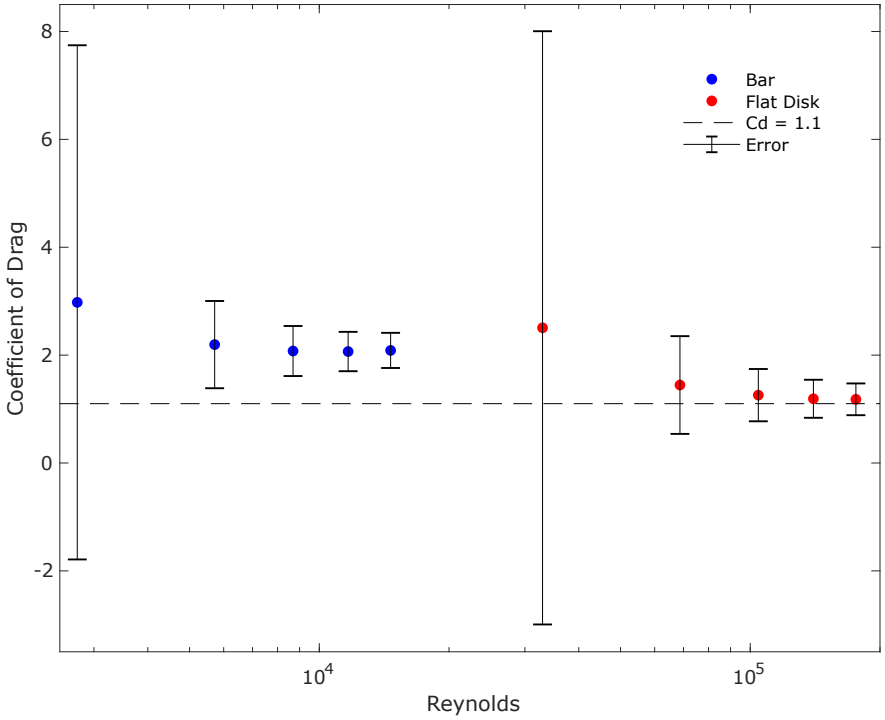

Figure 5.3: Non-dimensional drag data (C_D vs. Re) for bot the bar and flat disk with our measurement device. Error bars from uncertainty calculations are included with each point.

Analyzing the non-dimensional drag data and Fig. 5.3, we found that our calculations became more accurate as the velocity of the wind tunnel increased. The lower the velocity, the more sensitive the data became to small changes in force. Ideally, the coefficient of drag for a flat disk would be right around 1.1, which our data approach to within 10% at higher velocities. At the lowest velocity of 7.56 m/s, our coefficient of drag error was 127%; as the velocity reached 23.94 m/s, the error shrunk down to 9%, and at 40.32 m/s it was only 7.36%. At an error of 7.36%, we could attribute this deviation to small factors like material, surface roughness, etc. Our data for the bar appeared to follow the same pattern, becoming more accurate as the wind speed increased. From this, we assumed the ideal coefficient of drag for our object to be 2.0. This was encompassed in our calculated uncertainties.

6 Conclusions and Recommendations

Using a single strain gauge and cantilever beam as a device to measure drag on an object is simple to implement, but results in significant uncertainty at low velocities. At low wind velocities, drag and therefore strain in the deflected beam are very small. The small change in the strain gauge voltage output can be on the same order as the noise in the voltage

signal. At higher wind velocities, drag increases, resulting in less overall uncertainty in the calculated coefficient of drag.

Intrinsic defects in the construction of the measurement device lead to inaccurate measurements. A non-linear elastic region of the material will result in deviation from a linear fitted calibration curve. Small forces causing deflection of the beam must also overcome stiction in the material and between the adhesive and metal interface. Additionally, strain deviates from the ideal linear prediction if material defects, such as uneven beam thickness, exist in proximity to the strain gauge.

We recommend three principle improvements for related testing. First, the accuracy of the our measurement device can be improved by making modifications to the beam construction. Because more strain resulted in a coefficient of drag closer to the predicted value, a thinner beam with a more flexible material could be better suited for measuring drag within the range of Reynolds number tested. This holds as long as the modulus of elasticity is sufficiently large to avoid inelastic deformation after repeated use. Second, using a pitot probe, pressure transducer, force transducer, or any other specialized measuring device will help with the accuracy of data acquisition. Lastly, securing the measurement device and attached wires more securely (perhaps securing the device at multiple points) will decrease oscillations and resonance in the output force.

Appendix

A Reference Figures

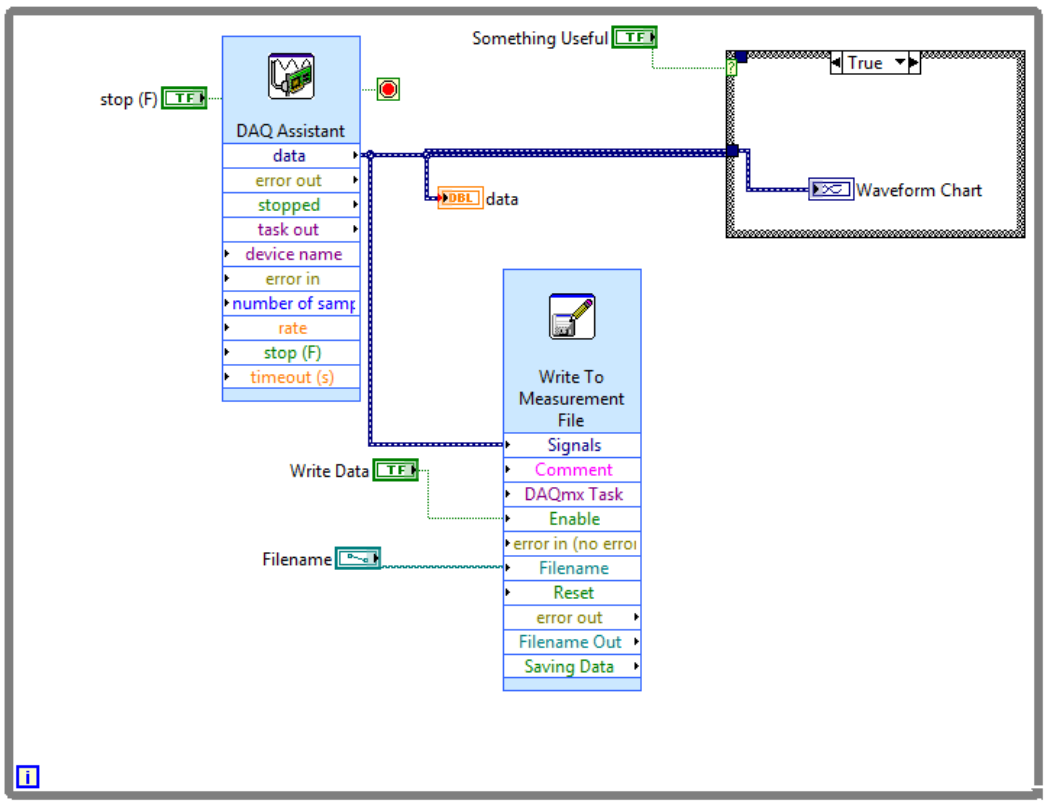

Figure A.1: Block diagram used to acquire data from various tests.

Figure A.2: Wheatstone bridge set up for signal conditioning. This specific set up is for a quarter bridge.

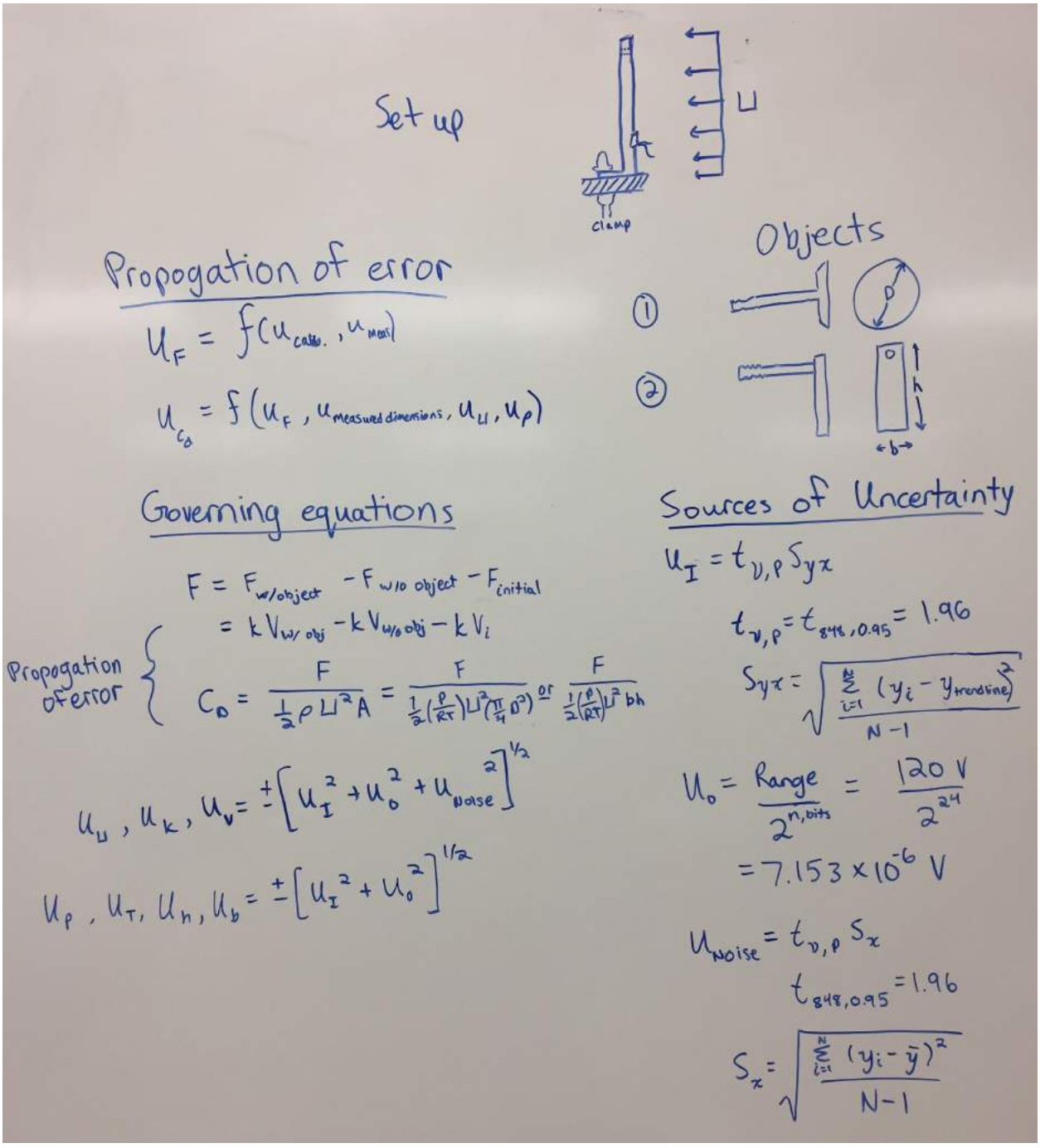

Figure A.3: Uncertainty Calculations.

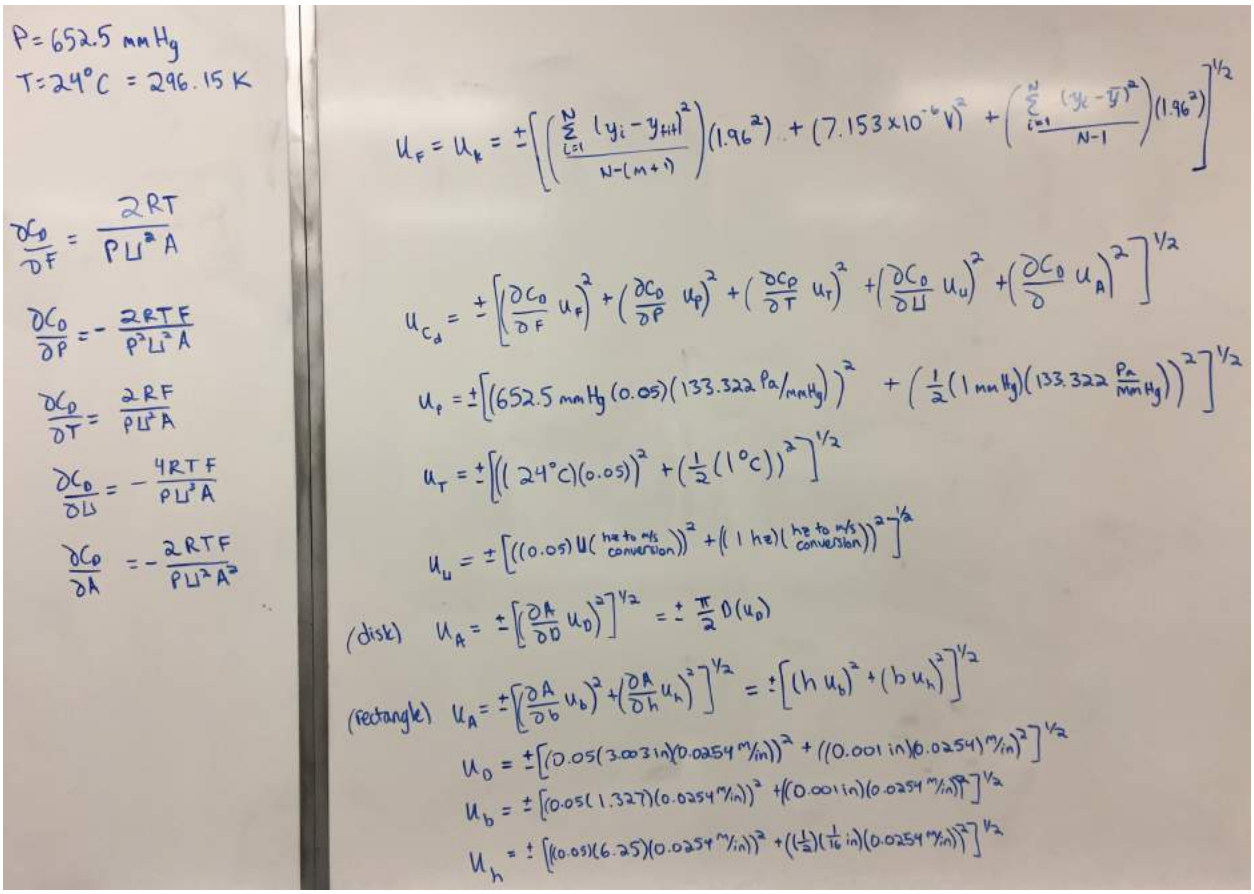

Figure A.4: Uncertainty Calculations.